

pubs.acs.org/JCTC Article

Impact of Local and Nonlocal Vibronic Coupling on the Absorption and Emission Spectra of J- and H-Dimers

Published as part of Journal of Chemical Theory and Computation virtual special issue "First-Principles Simulations of Molecular Optoelectronic Materials: Elementary Excitations and Spatiotemporal Dynamics".

Hamed Haghshenas and Frank C. Spano*



Cite This: https://doi.org/10.1021/acs.jctc.4c00299



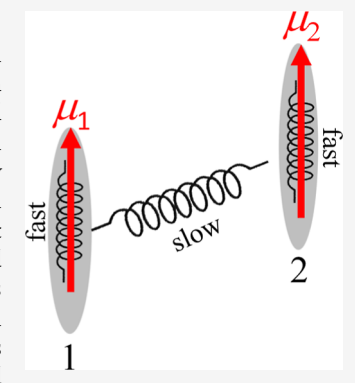
ACCESS

III Metrics & More

Article Recommendations

Supporting Information

ABSTRACT: The impact of exciton-vibrational (EV) coupling involving low-energy ("slow") intermolecular vibrations and higher-energy ("fast") intramolecular vibrations on the absorption and emission spectra of H- and J-dimers is studied theoretically for a pair of chromophores with excitonic coupling dominated by transition dipole—dipole coupling, J_C . Exact quantum-mechanical solutions based on a Frenkel—Holstein—Peierls Hamiltonian reveal a fascinating interplay between the two coupling sources in determining the spectral line widths, Stoke shifts and radiative decay rates. It is shown that the ratio rules derived from the vibronic progression of the fast mode in molecular dimers remain valid under the influence of slow-mode EV coupling under most conditions. However, a highly unusual aggregate behavior occurs when the product of local and nonlocal couplings, $|g_1g_{NL}|$, exceeds $2\hbar\omega_s|J_C|$, where $\hbar\omega_s$ is the energy of the slow mode. In this regime and when g_L and g_{NL} are in-phase, an H-dimer ($J_C > 0$) becomes strongly emissive and can even be super-radiant, while a J-dimer ($J_C < 0$) with out-of-phase g_L and g_{NL} values becomes subradiant. Such behaviors are in marked contrast to the predictions of Kasha theory and demonstrate the richness of the photophysical behavior regulting from EV coupling involving interplaying interplays and the production of the photophysical behavior regulting from EV coupling involving interplaying interplayed interplaying interplayed interplaying interplaying interplaying interplaying interplay interplaying interplayin



demonstrate the richness of the photophysical behavior resulting from EV coupling involving inter- and intramolecular vibrations.

1. INTRODUCTION

The coupling between Frenkel excitons and molecular vibrations, either intramolecular or intermolecular, is an enduring theme in the study of electronic excitations in organic molecular aggregates, crystals, and polymers, 1-31 as such coupling strongly impacts energy transport as well as basic photophysical properties such as absorption and photoluminescence. 1-3,8,12,22-30 Self-trapping of Frenkel excitons due to coupling between excitons and intermolecular vibrations (or lattice phonons) has been a subject of considerable interest since the pioneering works of Toyozawa, 1 Rashba, 2,3 and Sumi 4,5 and has been implicated as the primary mechanism for the broad, red-shifted emission in some J-aggregate-forming dyes.^{32–37} Strongly related to self-trapped excitons are excimers, where the latter are usually distinguished from the former by the involvement of charge-transfer (CT) states.³⁸⁻⁴³ For both self-trapped excitons and excimers, photoluminescence is characterized by a red-shifted, featureless emission with a low quantum yield.

We have long been interested in the impact of local excitonvibrational (EV) coupling involving *intra*molecular vibrations on the exciton absorption and photoluminescence (PL) line shapes in π -conjugated J- and H-molecular aggregates, where the vinyl-stretching mode with the energy of approximately 1400 cm⁻¹ manifests as pronounced vibronic progressions. Such progressions derive from the shift of the excited state (S_1) potential energy surface (PES) relative to the ground-state PES (S_0) . The shift is the source of local EV coupling in aggregates and is readily accounted for with a Frenkel-Holstein Hamiltonian. A set of ratio rules²³⁻²⁵ based on the aggregation-induced changes in the relative intensities of the first two vibronic peaks in the absorption and emission spectra was developed from which the exciton bandwidth and coherence length could be simply determined for both J- and H-aggregates. We have recently expanded our analysis to include local and nonlocal coupling to intermolecular vibrations⁴⁴ utilizing a Holstein-Peierls Hamiltonian.^{6,7,45,46} Generally, nonlocal coupling refers to the (first-order) change in the electronic coupling as the intermolecular mode evolves along the excited-state potential surface. In ref 44 and in many other works, nonlocal coupling pertains to the electron- and hole-transfer integrals. 12,46-49 Such nonlocal coupling modulates Frenkel-CT mixing and therefore impacts excimer emission. Applications of the theory presented in ref 44 to covalently bound perylene diimide dimers successfully

Received: March 7, 2024 Revised: May 2, 2024 Accepted: May 6, 2024



accounted for the unusual temperature dependence of the PL line shapes observed by Giaimo et al.⁵⁰

In the current work, we explore the impact of EV coupling to a low-frequency ("slow") intermolecular vibration on the absorption and photoluminescence (PL) line shapes of molecular dimers as a first step in eventually tackling larger aggregates in the context of self-trapping. We utilize a Frenkel-Holstein-Peierls Hamiltonian to simultaneously treat both local and nonlocal coupling and evaluate the spectral line shapes and radiative decay rates in J- and Hdimers. Here, nonlocal coupling is mainly derived from the change in Coulombic coupling induced by the slow-mode evolution, allowing a direct comparison of our results with the Kasha theory⁵¹⁻⁵³ of molecular J- and H-aggregates. We further include local coupling to the aforementioned highfrequency ("fast") vinyl-stretching mode in order to evaluate the robustness of the vibronic ratio rules^{23–25} in the presence of slow-mode coupling. The spectral simulations are based on exact quantum-mechanical treatment of the Hamiltonian; we do not invoke any adiabatic approximations. Overall, we find that the ratio rules derived earlier when only the fast mode is present remain valid when slow-mode local and nonlocal couplings are activated. We also show how the constructive and destructive interference between the local and nonlocal couplings involving the slow mode impact the absorption and PL spectral line shapes and shifts. In the most extreme cases, such interference can lead to highly unusual superemissive Haggregates and subradiant J-aggregates.

2. METHODS

In what follows, we consider molecular aggregates composed of two identical chromophores related via a symmetry operation. Each chromophore hosts an electronic ground state (S_0) and an electronic excited state (S_1) . The dimer undergoes "fast" intramolecular and "slow" intermolecular vibrations, as depicted in Figure 1. The fast mode with energy

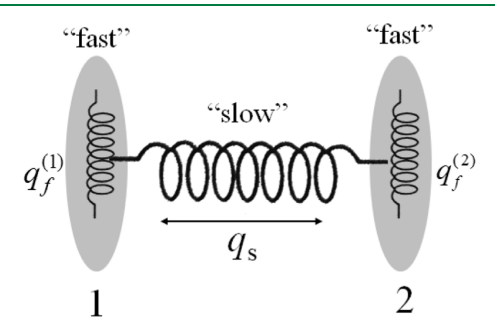


Figure 1. Molecular dimer depicting "fast" intramolecular and "slow" intermolecular vibrations.

 $\hbar\omega_{\rm f}\approx 1400~{\rm cm}^{-1}$ accounts for the pronounced vibronic progressions observed in the absorption and PL spectra of many π -conjugated molecules and is derived from vinyl- (or aromatic-quinoidal) stretching motion. Here, and in all that follows, energy is expressed in units of wave numbers (cm⁻¹). In order to simplify the notation, we further set $\hbar=1$ so that $\omega_{\rm f}$ represents the fast-mode energy (in units of wave numbers). In the simplest approach, local EV coupling for the fast mode is described using shifted harmonic S₀ and S₁ potential energy surfaces (PESs) of identical curvature, as depicted in Figure 2a. The fast-mode nuclear coordinate is denoted as $q_{\rm f}$ and describes single-bond shortening and double-bond lengthening

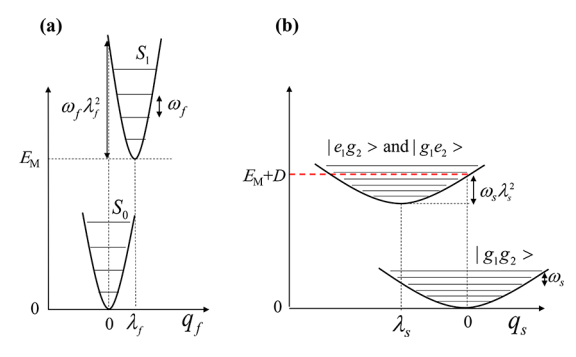


Figure 2. (a) Single-chromophore ground-state PES (S_0) and excited-state PES (S_1) as a function of the fast, intramolecular coordinate q_E . (b) Ground-state PES $(|g_1g_2\rangle)$ and excited-state PES (for either $|e_1g_2\rangle$ or $|g_1e_2\rangle$) as a function of the slow-mode coordinate q_s , The excited PES incorporate local coupling described using λ_s , which is equal to $-g_L/2\omega_s$ (see text).

in the course of the oscillation. The displacement of the S_1 PES is quantified by the Huang–Rhys (HR) factor, λ_f^2 , which is typically between 0.5 and 1.5 for most organic chromophores. The monomer transition energy, $E_{\rm M}$, is associated with the 0–0 transition in Figure 2a.

Within each dimer, a slow, symmetry-preserving intermolecular vibration is also included. The mode frequency is typically in the terahertz range, with the mode energy in the range, $\omega_s = 10-100 \text{ cm}^{-1}$. The intermolecular coordinate is denoted as q_s and can represent, for example, the deviation of the distance between the two molecular mass centers relative to the ground-state minimum (defined as $q_s = 0$). The PES for the ground electronic state, $|g_1,g_2\rangle$, where both chromophores are in the state S_0 , is taken to be harmonic in the slow-mode coordinate q_s , as depicted in Figure 2b. The figure also shows the excited-state PES which represents both $|e_1g_2\rangle$ and $|g_1e_2\rangle$ and is taken to have the same curvature as the ground state well. The shift and relaxation due to local EV coupling are described with the HR factor λ_s^2 , which is further discussed below. The excitation energy in the dimer is $E_{\rm M}$ + D, where Dis the gas-to-crystal red shift due to nonresonant coupling

between an excited- and ground-state chromophore. Finally, as in the Kasha model, $^{51-53}$ resonant energy transfer between the states $|e_1g_2\rangle$ and $|g_1e_2\rangle$ occurs via transition dipole—dipole coupling, $J_{\rm C}$, Changes in $J_{\rm C}$ due to motion along the slow-mode coordinate, $q_{\rm s}$ —known as nonlocal coupling—is also accounted for. Overall, we are interested in how the absorption and emission spectra in H-aggregates ($J_{\rm C}>0$) and J-aggregates ($J_{\rm C}<0$) are impacted by local and nonlocal EV coupling to the slow-vibrational mode in the presence of local coupling to the fast mode.

All of the above processes can be represented by a Frenkel–Holstein–Peierls Hamiltonian, expressed as

$$H_{\rm FHP} = H_{\rm F} + H_{\rm s}^{\rm vib} + H_{\rm f}^{\rm vib} \tag{1}$$

The first term is the Frenkel Hamiltonian, H_F , which accounts for the nonresonant spectral shift (D) and resonant Coulomb coupling (J_C) between the two chromophores

$$H_{\rm F} = (E_{\rm M} + D) \sum_{n=1,2} |n\rangle\langle n| + J_{\rm C} \{|1\rangle\langle 2| + |2\rangle\langle 1|\}$$
 (2)

Here, the state $|n\rangle$ indicates that the n th chromophore (n=1, 2) hosts a local excitation (S_1), while the other chromophore remains unexcited (S_0). For example, $|n=1\rangle = |e_1g_2\rangle$.

Generally, D and J_C depend on q_s , i.e. $D(q_s)$ and $J_C(q_s)$. The values in eq 2 correspond to the ground-state geometry, $q_s = 0$, i.e., $D \equiv D(0)$ and $J_C \equiv J_C(0)$. While D is usually a negative quantity inducing a gas-to-crystal red-shift, J_C is positive (negative) for H-aggregates (J-aggregates). Diagonalizing H_F results in the two delocalized Frenkel exciton (FE) eigenstates

$$|k\rangle \equiv 2^{-1/2} \{|1\rangle + e^{ik}|2\rangle\} \qquad k = 0, \pi$$

with wave vector k and with energies

$$E_{\rm F}(k) = E_{\rm M} + D + J_{\rm C}\cos(k) \tag{4}$$

The k wave vector notation is useful in comparing the dimer in this work to larger π -stacks with one molecule per unit cell treated in previous works, where translational symmetry leads to a good quantum number, k, which ranges over the Brillouin zone. The phases of the local states, $|1\rangle$ and $|2\rangle$, are chosen such that their $S_0 \to S_1$ molecular transition dipole moments are parallel and aligned. As such, the k=0 state carries all of the oscillator strength. Furthermore, the symmetry-preserving slow mode maintains the alignment.

The impact of the slow *inter*molecular mode is contained in H_s^{vib} , with

$$H_{\rm s}^{\rm vib} = \omega_{\rm s} \beta^{\dagger} \beta + g_{\rm L} \hat{q}_{\rm s} \sum_{n} |n\rangle \langle n| + g_{\rm NL} \hat{q}_{\rm s} \{|1\rangle \langle 2| + |2\rangle \langle 1|\}$$
(5)

The first term represents the mode energy (taking $\hbar=1$). $\beta^{\dagger}(\beta)$ is the creation (annihilation) operator for a slow-mode vibrational quantum in the ground-state potential well. (Note that we have neglected the offset of $(1/2)\omega_s$ found in the harmonic oscillator Hamiltonian since the common offset cancels out in all transition energies and has no impact on the absorption or emission spectra.) The second and third terms in eq 5 represent local (Holstein) and nonlocal (Peierls) vibronic coupling, respectively, with \hat{q}_s being the dimensionless operator representing the slow-mode coordinate. For example, if x_s is the distance between mass centers (relative to the equilibrium distance in the ground state), then, the dimensionless coordinate q_s is

$$q_{s} \equiv \sqrt{\frac{\pi m c \omega_{s}}{\hbar}} x_{s} \tag{6}$$

where m is the reduced mass of each chromophore, and ω_s is the mode energy in units of wave numbers. The operator form of q_s is then

$$\hat{q}_{s} \equiv \sqrt{\frac{\pi m c \omega_{s}}{\hbar}} \hat{x}_{s} = \frac{\beta^{\dagger} + \beta}{2} \tag{7}$$

The form of \hat{q}_s is consistent with our previous work.⁴⁴

The second term in eq 5 represents local coupling and arises from the first-order change in the nonresonant shift with q_s , i.e. $g_L \equiv [\mathrm{d}D(q_s)/\mathrm{d}q_s]_{q_s=0}$. Note that g_L has units of energy. Local coupling is diagonal in the $|n\rangle\langle n|$ space and can be exactly accounted for (in the absence of nonlocal coupling) by "completing the square" in the $|1\rangle\langle 1\rangle$ and $|2\rangle\langle 2|$ subspaces. The result is an excited-state PES which remains harmonic, but is shifted by $\lambda_s = -g_L/2\omega_s$, relative to the ground state, as depicted in Figure 2b for the case, $g_L > 0$. For a slow-mode stretching mode, g_L is positive, since the red-shifted D becomes less negative as the interchromophore distance increases. (However, other modes, for example, torsional modes, may yield negative values of g_L .)

The nonlocal coupling term in eq 5 is quantified by $g_{\rm NL}$ and accounts for the first-order change in the Coulomb coupling with $q_{\rm s'}$ i.e. $g_{\rm NL} \equiv \left[{\rm d}J_{\rm C}(q_{\rm s})/{\rm d}q_{\rm s}\right]_{q_{\rm S}=0}$. $g_{\rm NL}$ depends on the ground-state dimer geometry which differs for H- and J-aggregates. The former adopts a side-by-side configuration, while the latter adopts a head-to-tail configuration. If $q_{\rm s}$ corresponds to an intermolecular stretch along a line connecting the mass centers, then for H-aggregates ($J_{\rm C}>0$), the Coulomb coupling decreases with increasing $q_{\rm s}$ so that $g_{\rm NL}<0$, while for J-aggregates ($J_{\rm C}<0$) the Coulomb coupling becomes less negative with increasing $q_{\rm s}$ so that $g_{\rm NL}>0$. Assuming a point-dipole approximation for $J_{\rm C}$, where $J_{\rm C}$ scales as $1/(x_0+x_{\rm s})^3$, we obtain

$$g_{\rm NL} = \frac{\mathrm{d}x_{\rm s}}{\mathrm{d}q_{\rm s}} \times \frac{\mathrm{d}J_{\rm C}}{\mathrm{d}x_{\rm s}}|_{x_{\rm s}=0} = -\frac{3J_{\rm C}}{x_{\rm 0}} \sqrt{\hbar/\pi mc\omega_{\rm s}}$$
(8)

where x_0 is the equilibrium intermolecular separation. Assuming perylene $(C_{20}H_{12})$ chromophores with a reduced mass of approximately m=126 g/mol, along with $x_0=0.4$ nm and $\omega_s=100$ cm⁻¹, gives $g_{\rm NL}=-0.055J_{\rm C}$. For an H-aggregate with $J_{\rm C}=1000$ cm⁻¹, $g_{\rm NL}$ is then ≈-55 cm⁻¹. $g_{\rm NL}$ increases further as the mass, m, and mode frequency, ω_s , are reduced. For example, maintaining $J_{\rm C}=1000$ cm⁻¹ and reducing both m and ω_s by a factor of 4 give $|g_{\rm NL}|\approx200$ cm⁻¹. However, if the exciton coupling is generalized to also include $J_{\rm CT}$ (due to Frenkel–CT mixing 23,55), the values of $|g_{\rm NL}|$ can be much greater due to the strong sensitivity of the electron- and hole-transfer integrals to intermolecular separation. 56

Finally, the last term in eq 1 represents the vibrational energy of the aforementioned fast *intra*molecular vibration with mode energy $\omega_{\rm f}$ (=1400 cm⁻¹) along with its associated *local* vibronic coupling

$$H_{\rm f}^{\rm vib} = \omega_{\rm f} \sum_{n=1}^{2} b_n^{\dagger} b_n - \lambda_{\rm f} \omega_{\rm f} \sum_{n} (b_n^{\dagger} + b_n - \lambda_{\rm f}) |n\rangle \langle n|$$
 (9)

with b_n^{\dagger} (b_n) the creation (annihilation) operator for a fast-mode vibrational quantum in the ground-state potential well of molecule n. Including only a single intramolecular mode with energy approximately 1400 cm⁻¹ is usually all that is required to obtain excellent fits to the vibronic progressions appearing in the absorption and PL spectra of single chromophores; see, for example, ref 44.

2.1. Slow-Mode Coupling Only. Without the presence of the fast mode, the eigenstates and energies of Hamiltonian, $H_{\rm F}$ + $H_{\rm s}^{\rm vib}$, can be obtained exactly. After representing the Hamiltonian, $H_{\rm F}$ + $H_{\rm s}^{\rm vib}$ in the exciton basis, $|k\rangle$, it takes the form

$$\begin{split} H_{\rm F} + H_{\rm s}^{\rm vib} &= \omega_{\rm g} \beta^\dagger \beta |G\rangle \langle G| + \left\{ E_{\rm F}(0) + \omega_{\rm g} \tilde{\beta}_0^\dagger \tilde{\beta}_0 \right. \\ &\left. - \frac{\left(g_{\rm NL} + g_{\rm L} \right)^2}{4\omega_{\rm s}} \right\} |k=0\rangle \langle k=0| \\ &\left. + \left\{ E_{\rm F}(\pi) + \omega_{\rm g} \tilde{\beta}_\pi^\dagger \tilde{\beta}_\pi - \frac{\left(g_{\rm NL} - g_{\rm L} \right)^2}{4\omega_{\rm s}} \right\} |k=\pi\rangle \langle k=\pi| \end{split}$$

where we have introduced the electronic ground state $|G\rangle \equiv |g_1g_2\rangle$ in which both chromophores are in their ground (S_0) electronic states. The first term in eq 10 accounts for the

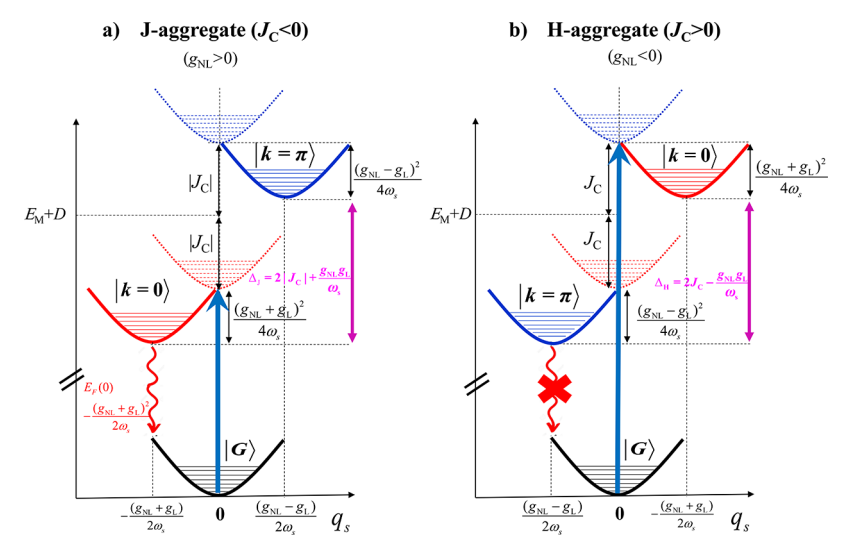


Figure 3. (a) J-dimer and (b) H-dimer harmonic PESs for the ground and excited states before (dotted) and after (solid) the activation of slow-mode local and nonlocal coupling. The k = 0 ($k = \pi$) wells are indicated in red (blue). Blue arrows indicate absorption while red wavy lines indicate emission. Purple double arrow indicates the interwell separation. The diagrams assume $|g_{NL}| \gg |g_L|$ to emphasize the opposing directional shifts of the k = 0 and $k = \pi$ wells due to nonlocal coupling. In the opposite limit $|g_L| \gg |g_{NL}|$ (not shown), the two wells undergo unidirectional shifts.

energy of the slow-mode vibrational excitations which occur in the (unshifted) ground-state harmonic well depicted in Figure 2b. In the excited-state subspace (second and third terms in eq 10), the associated slow-mode creation operators corresponding to the k=0 and $k=\pi$ harmonic wells are given by the shifted operators

$$\tilde{\beta}_0^{\dagger} \equiv \beta^{\dagger} + (g_L + g_{NL})/2\omega_s \tag{11a}$$

and

$$\tilde{\beta}_{\pi}^{\dagger} \equiv \beta^{\dagger} + (g_{L} - g_{NL})/2\omega_{s} \tag{11b}$$

with the corresponding destruction operators obtained via Hermitian conjugation.

According to eqs 10 and 11, the excited-state PES's take the form of shifted and relaxed harmonic wells, where the well positions depend on the interference between the local and nonlocal coupling. Although local coupling induces *uniformly* shifted wells by $-g_{\rm L}/2\omega_{\rm s}$ for both k=0 and $k=\pi$ excitons, nonlocal coupling induces *oppositely* shifted wells; $-g_{\rm NL}/2\omega_{\rm s}$ for the k=0 well and $+g_{\rm NL}/2\omega_{\rm s}$ for the $k=\pi$ well. The excited eigenstates within the kth well are given by $|k; \tilde{v}_{\rm s}\rangle$, where $\tilde{v}_{\rm s}=0$, 1, 2, \cdots is the number of slow-mode vibrational quanta. The associated energies are

$$E_{k,\tilde{v}_{s}} = E_{M} + D + J_{C}\cos k - (g_{NL} + e^{ik}g_{L})^{2}/4\omega_{s} + \tilde{v}_{s}\omega_{s}$$
(12)

Finally, eigenstates in the electronic ground-state potential with ν_s quanta of slow-mode vibrations are denoted as $|G;\nu_s\rangle$ ($\nu_s=0,1,2,\ldots$) with energies, $E_{G;\nu_s}=\nu_s\omega_s$. (The ground electronic energy is taken to be zero.)

The excited-state potential energy wells before (dotted) and after (solid) the activation of local and nonlocal couplings are depicted in Figure 3a,b for J-aggregates ($J_{\rm C} < 0$, $g_{\rm NL} > 0$) and H-aggregates ($J_{\rm C} > 0$, $g_{\rm NL} < 0$). The figure shows that the k=0 and $k=\pi$ wells shift by $-(g_{\rm L}+g_{\rm NL})/2\omega_s$ and $-(g_{\rm L}-g_{\rm NL})/2\omega_s$, respectively, with the corresponding relaxation energies ($g_{\rm L}+g_{\rm NL})^2/4\omega_s$ and ($g_{\rm L}-g_{\rm NL})^2/4\omega_s$. The figure portrays the case where the nonlocal coupling is dominant ($|g_{\rm NL}| \gg |g_{\rm L}|$) so that

the k=0 and $k=\pi$ harmonic wells mainly shift in *opposite* directions, with both potentials undergoing a relaxation energy approximately equal to $g_{\rm NL}^2/4\omega_s$. The barrier-free relaxation seen here for dimers is the origin of self-trapping in larger aggregates. Opposing well shifts induced by nonlocal coupling have been shown before, for the case of charge carriers by Coropceanu et al. Figure 3 shows that when the dominant nonlocal coupling is associated with an intermolecular stretching mode, the bright state (k=0) contracts along q_s in a J-dimer but expands along q_s in an H-dimer. The opposite shift is realized by the $k=\pi$ well.

Figure 3 reveals an interesting interference between local and nonlocal couplings. For the k=0 well, which dictates absorption, the overall shift and relaxation depend on the sum $g_{\rm NL}+g_{\rm L}$ so that destructive interference occurs when $g_{\rm NL}$ and $g_{\rm L}$ have opposite signs. The destructive interference is complete when $g_{\rm NL}=-g_{\rm L}$, and the k=0 well undergoes no shift and therefore no relaxation at all. This is demonstrated in Figure 4a for the k=0 well in a J-aggregate. Conversely, constructive interference occurs when the two coupling constants have the same sign, as demonstrated in Figure 4b. In this case, the shift and relaxation energy of the k=0 well are greatly enhanced. Unlike the k=0 well, the shift of the $k=\pi$ well is governed by the difference, $g_{\rm L}-g_{\rm NL}$. As we will see in the following section, the interferences in both wells profoundly affect the absorption and PL line shapes.

Because the k=0 and $k=\pi$ wells respond to $g_{\rm NL}+g_{\rm L}$ and $g_{\rm NL}-g_{\rm L}$, respectively, the energy difference between the two wells changes whenever $g_{\rm L}$ and $g_{\rm NL}$ are both nonzero. For J- and H-dimers, the vertical (or energetic) separation between wells is defined as

$$\Delta_{\rm J} \equiv E_{k=\pi,0} - E_{k=0,0} = 2|J_{\rm C}| + \frac{g_{\rm NL}g_{\rm L}}{\omega_{\rm s}} \eqno(13a)$$

$$\Delta_{\rm H} \equiv E_{k=0,0} - E_{k=\pi,0} = 2J_{\rm C} - \frac{g_{\rm NL}g_{\rm L}}{\omega_{\rm s}}$$
(13b)

where eq 12 was used to resolve the energies, $E_{k,0}$. The interwell separation is indicated by the purple arrows in Figure

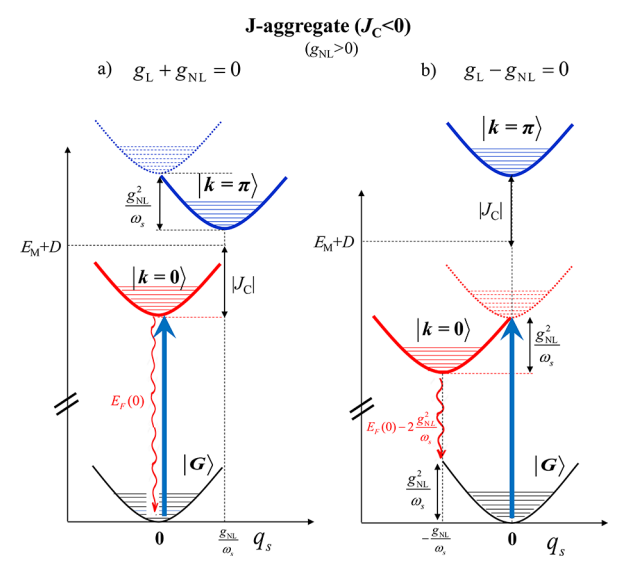


Figure 4. Harmonic PESs for the ground and excited states in a J-dimer before (dotted) and after (solid) activation of slow-mode coupling when (a) $g_{\rm L}$ and $g_{\rm NL}$ destructively interfere and (b) when they constructively interfere.

3. When the product $g_{\rm NL}g_{\rm L}$ is zero, the interwell separation in both H- and J-dimers is simply the exciton bandwidth, $2|J_{\rm C}|$. However, in a J-dimer, $\Delta_{\rm J}$ decreases (increases) if $g_{\rm NL}g_{\rm L}$ is negative (positive). When

$$g_{NL}g_{L} < -2|J_{C}|\omega_{s}$$
, (subradiant J-dimer) (14a)

 Δ_J falls below zero, resulting in an energetic reordering of the two wells. In this exotic regime, the dimer will absorb as a Jaggregate but will emit like an H-aggregate, i.e., a subradiant Jaggregate. Conversely, for an H-dimer, Δ_H decreases (increases) if $g_{NL}g_L$ is positive (negative). Energetic reordering of the two wells $(\Delta_H < 0)$ occurs when

$$g_{NI}g_{L} > 2J_{C}\omega_{s}$$
 (super-emissive H-dimers) (14b)

leading to an H-aggregate with respect to absorption but a J-aggregate with respect to PL, i.e., a superemissive H-aggregate.

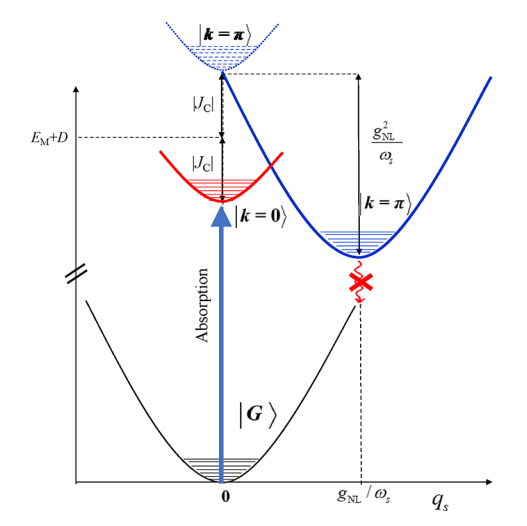
The simplest case to appreciate such unorthodox J- and H-dimers is when $|g_{\rm NL}| = |g_{\rm L}|$, as demonstrated in Figure 5a,b. For the J-dimer with $g_{\rm NL} = -g_{\rm L}$, the k=0 well does not shift or relax, but the $k=\pi$ well relaxes by $(g_{\rm NL}-g_{\rm L})^2/4\omega_{\rm s}=g_{\rm NL}^2/\omega_{\rm s}$. Hence, $\Delta_{\rm J}$ becomes negative when $g_{\rm NL}^2/\omega_{\rm s}>2|J_{\rm C}|$. Interestingly, the aggregate absorption peak is still red-shifted relative to the monomer, as indicated by the blue arrow in Figure 5a, but the emission, which originates from the lowest-energy excited state (Kasha's rule⁵⁷), is now forbidden, at least at T=0 K. Thermally activated emission is of course possible (see the following section). Conversely, for the H-dimer in Figure 5b, with $g_{\rm NL}=g_{\rm L}$, the $k=\pi$ well does not shift or relax, but the $k=\pi$ well relaxes by $(g_{\rm NL}-g_{\rm L})^2/4\omega_{\rm s}=g_{\rm NL}^2/\omega_{\rm s}$. Hence, $\Delta_{\rm H}$ becomes negative when $g_{\rm NL}^2/\omega_{\rm s}>2J_{\rm C}$. The aggregate absorption peak is still blue-shifted relative to the monomer, as indicated by the blue arrow in Figure 5b, but the emission is now superradiantly enhanced.

2.2. General Case: Fast and Slow Modes. We now include local coupling to the fast mode and consider the complete Hamiltonian in eq 1. Additional terms beyond those in eq 10 are obtained after expressing $H_{\rm f}^{\rm vib}$ in the electronic basis set spanned by $|{\rm G}\rangle$, $|k=0\rangle$ and $|k=\pi\rangle$, resulting in

$$\begin{split} H_{\rm FHP} &= H_{\rm F} + H_{\rm s}^{\rm vib} + \omega_{\rm f} \sum_{q=0,\pi} b_q^\dagger b_q |G\rangle \langle G| \\ &+ \left\{ \omega_{\rm f} \tilde{b}_{q=0}^\dagger \tilde{b}_{q=0} + \omega_{\rm f} b_{q=\pi}^\dagger b_{q=\pi} + \frac{1}{2} \omega_{\rm f} \lambda_{\rm f}^2 \right\} |k=0\rangle \langle k=0| \\ &+ \left\{ \omega_{\rm f} \tilde{b}_{q=0}^\dagger \tilde{b}_{q=0} + \omega_{\rm f} b_{q=\pi}^\dagger b_{q=\pi} + \frac{1}{2} \omega_{\rm f} \lambda_{\rm f}^2 \right\} |k=\pi\rangle \langle k=\pi| \\ &- \frac{\lambda_{\rm f} \omega_{\rm f}}{\sqrt{2}} (b_{q=\pi}^\dagger + b_{q=\pi}) \{ |k=0\rangle \langle k=\pi| + |k=\pi\rangle \langle k=0| \} \end{split} \label{eq:heaviside}$$

a) Non-emissive J-aggregate $(J_C < 0)$

$$g_{\rm NL}g_{\rm L} < -2 \mid J_{\rm C} \mid \omega_{\rm s}$$
$$(g_{\rm NL} = -g_{\rm L} > 0)$$



Emissive H-aggregate $(J_C>0)$

b)

$$g_{\rm NL}g_{\rm L} > 2J_{\rm C}\omega_{\rm s}$$
 $(g_{\rm NL} = g_{\rm L} < 0)$

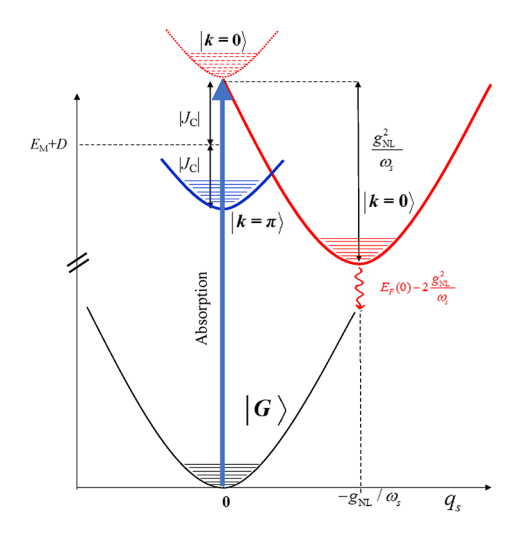


Figure 5. Harmonic PESs for the ground and excited states in (a) subradiant J-dimer where Δ_{J} < 0 and (b) emissive H-dimer, where Δ_{H} < 0. When T = 0 K emission originates from the lowest-energy excited state.

where we have introduced the fast-mode phonon creation operators with wave vector q, as

$$b_{q=0}^{\dagger} \equiv (b_1^{\dagger} + b_2^{\dagger})/\sqrt{2} \tag{16a}$$

and

$$b_{q=\pi}^{\dagger} \equiv (b_1^{\dagger} - b_2^{\dagger})/\sqrt{2} \tag{16b}$$

The Hamiltonian includes the totally symmetric vibration (q = 0) which is shifted by $\lambda_f / \sqrt{2}$.²⁵

$$\tilde{b}_{q=0}^{\dagger} \equiv b_{q=0}^{\dagger} - \lambda_{\rm f} / \sqrt{2} \tag{16c}$$

as indicated by the tilde overstrike. Most importantly, the last term in eq 15 couples the k = 0 and $k = \pi$ subspaces, thereby complicating the evaluation of the eigenstates and energies.

With the form of the Hamiltonian given by eq 15, it proves convenient to expand the excited-state wave functions in the exciton—phonon basis set, as was done in ref^{2.5}

$$\begin{split} |\Psi_{\text{ex}}^{(\kappa,i)}\rangle &= \sum_{k} \sum_{\tilde{n}_{q=0}} \sum_{n_{q=\pi}} \sum_{\tilde{n}_{s,k}}' c_{k,\tilde{n}_{q=0},n_{q=\pi},\tilde{n}_{s,k}}^{(i)} \\ &\times |k> \otimes |\tilde{n}_{q=0}, n_{q=\pi}\rangle \otimes |\tilde{n}_{s,k}\rangle \end{split} \tag{17}$$

where the phonon number states are eigenstates of the number operator. For the fast modes

$$\tilde{b}_{q=0}^{\dagger} \tilde{b}_{q=0} | \tilde{n}_{q=0}, \ n_{q=\pi} \rangle = \tilde{n}_{q=0} | \tilde{n}_{q=0}, \ n_{q=\pi} \rangle$$
(18a)

and

$$b_{q=\pi}^{\dagger}b_{q=\pi}|\tilde{n}_{q=0}, n_{q=\pi}\rangle = n_{q=\pi}|\tilde{n}_{q=0}, n_{q=\pi}\rangle$$
 (18b)

with $\tilde{n}_{q=0}, n_{q=\pi} = 0,1,2,\cdots$, while for the slow mode

$$\tilde{\beta}_{k}^{\dagger} \tilde{\beta}_{k} | \tilde{n}_{s,k} \rangle = \tilde{n}_{s,k} | \tilde{n}_{s,k} \rangle, \qquad \tilde{n}_{s,k} = 0, 1, 2, \dots$$
(18c)

We emphasize that the exciton (k) and phonon (q) wavevectors are not individually good quantum numbers because of the last term in eq 15. Instead, the total wavevector

$$\kappa = k + n_{a=\pi} \pi \tag{19}$$

is a good quantum number (modulo 2π). Hence, the *i*th eigenfunction with κ (=0, π) in eq 17, $|\Psi_{ex}^{(\kappa,i)}\rangle$, is expanded in basis states with like values of κ , as indicated by the prime on the summations. For example, for the *i*th eigenstate with total momentum, $\kappa = \pi$, only basis states with k = 0 and $n_{q=\pi} = 1$, 3, ... as well as states with $k = \pi$ and $n_{q=\pi} = 0.2.4$, ... are included in the summations. Note that slow-mode coupling is confined to a single, symmetric vibration and therefore has no effect on κ .

Finally, the electronic ground states are expressed as

$$|\Psi_{G,n_{q=0},n_{q=\pi},n_{s,G}}\rangle = |G> \otimes |n_{q=0},n_{q=\pi}\rangle \otimes |n_{s,G}\rangle \tag{20a}$$

with energies

$$E_{G,n_{q=0},n_{q=\pi},n_{s}} = (n_{q=0} + n_{q=\pi})\omega_{f} + n_{s,G}\omega_{s}$$
 (20b)

In this case, all vibrational quanta refer to unshifted potentials (no tilde overstrike) as in the ground-state harmonic wells in Figure 3.

To numerically evaluate the excited-state eigenvectors and eigenvalues of the Hamiltonian in eq 15, we utilized the exciton—phonon basis set, capping the total number of fast-mode vibrational quanta at 5 and the number of slow-mode vibrational quanta at 200. These values were high enough to

ensure convergence in the computed optical spectra in the following section.

3. RESULTS: ABSORPTION AND PL

In this section, we evaluate the impact of local and nonlocal EV coupling on the steady-state absorption and photoluminescence spectra of J- and H-dimers. At T=0 K, so that only the lowest-energy ground-state $|\Psi_{G,0,0,0}\rangle$ is populated, the absorption spectrum is given by

$$A(\omega) = \sum_{i} |\langle \Psi_{G,0,0,0} | \hat{\mu} | \Psi_{\text{ex}}^{(\kappa=0,i)} \rangle|^2 W(\omega - \omega_{\kappa=0,i})$$
(21)

where the electronic transition dipole moment (tdm) operator is $\hat{\mu} = \mu \sum_{n=1,2} \{ |n\rangle \langle G| + |G\rangle \langle n| \}$, with μ being the molecular tdm. (We assume the molecular tdm's remain aligned during the slow-mode vibration.) The transition dipole moment is nonzero only for the $\kappa = 0$ eigenstates, as indicated in eq 21. The homogeneous line shape function is taken to be a peak-normalized Gaussian

$$W(\omega) = \exp(-\omega^2/2\sigma_{\rm H}^2) \tag{22}$$

with standard deviation, $\sigma_{\rm H}$. One can also take a Lorentzian line shape; the particular form does not impact any of the main conclusions reached in the present paper.

At T=0 K, PL originates from just the lowest-energy eigenstate, $|\Psi_{\rm em}\rangle$, of the Hamiltonian in eq 15 with energy, E_{em} . Emission consists of a series of transitions, with each transition distinguished by its terminal electronic ground state, $|\Psi_{G,n_{q=0},n_{q=m},n_{s,G}}\rangle$, specified by the number of fast- and slow-mode vibrational quanta in the ground-state potential wells. The PL spectrum takes the form

$$S(\omega) = \sum_{n_{q=0}} \sum_{n_{q=x}} \sum_{n_{s}} |\langle \Psi_{G,n_{q=0},n_{q=x},n_{s,G}} | \hat{\mu} | \Psi_{em} \rangle|^{2}$$

$$\times W(\omega - E_{em} + E_{G,n_{q=0},n_{q=x},n_{s,G}})$$
(23)

eq 23 is referred to as the *reduced* PL spectrum since it omits the cubic transition frequency term normally found in the Einstein expression for spontaneous emission. In this way, the vibronic peaks are dictated entirely by FC factors, allowing for simple vibronic ratio rules.^{23–25} For higher temperatures, the absorption spectrum in eq 21 is averaged over a Boltzmann distribution of "hot" ground states, while the PL spectrum in eq 23 is averaged over a Boltzmann distribution of thermally relaxed excited states; see eqs S.1 and S.2.

Finally, we consider the radiative decay rate. In general, the radiative decay rate for the dimer, $\gamma_{\rm D}$, is computed by evaluating the Einstein radiative rate for each emission transition and then summing over all transitions. At T=0 K, $\gamma_{\rm D}$ is

$$\gamma_{\rm D} = \frac{n}{3\pi\varepsilon_0 \hbar^4 c^3} \sum_{n_{q=0}} \sum_{n_{q=\pi}} \sum_{n_{s,G}} (E_{\rm em} - E_{G,n_{q=0},n_{q=\pi},n_{s,G}})^3 \times |\langle \Psi_{\rm em}|\hat{\mu}|\Psi_{G,n_{q=0},n_{q=\pi},n_{s,G}}\rangle|^2$$
(24)

where n is the index of refraction, ε_0 is the permittivity of free space, and c is the speed of light. The expression for a general temperature T is given in eq S.3. Furthermore, for a single chromophore (monomer), the radiative decay rate, $\gamma_{\rm M}$, is given by

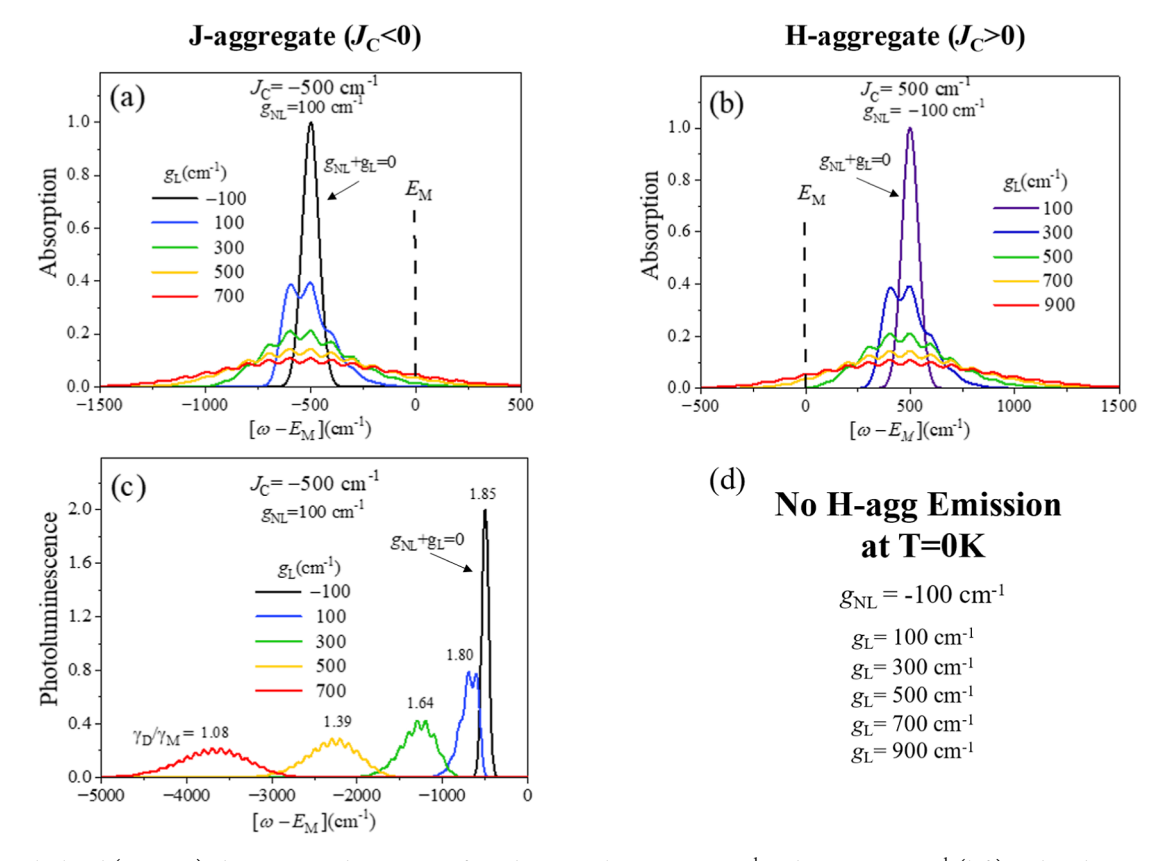


Figure 6. Calculated (T=0 K) absorption and PL spectra for J-dimers with J=-500 cm⁻¹ and $g_{\rm NL}=100$ cm⁻¹ (left) and H-dimers with J=500 cm⁻¹ and $g_{\rm NL}=-100$ cm⁻¹ (right) from eqs 21 and 23 based on the Hamiltonian in eq 10 with $ω_{\rm s}=100$ cm⁻¹. Spectra are shown for several values of local coupling, $g_{\rm L}$. The H-/J-dependent signs of $g_{\rm NL}$ as well as positive values for $g_{\rm L}$ are consistent with a stretching mode (see text). The "reduced" spectra are calculated without the transition frequency factor; for example, the cubic dependence on the transition frequency is omitted in the PL spectra in order to better focus on the vibronic contributions. Fast-mode EV coupling is neglected. In order to resolve the slow-mode vibronic structure, the homogeneous line width is set to $σ_{\rm H}=40$ cm⁻¹.

$$\gamma_{\rm M} = \frac{n\mu^2}{3\pi\epsilon_0 \hbar^4 c^3} \sum_{\nu=0,1,2,\dots} (E_{\rm M} - \nu \omega_{\rm f})^3 \frac{e^{-\lambda^2 \lambda^{2\nu}}}{\nu!}$$
(25)

For the dimer, we further define the dimensionless emission strength, $I_{\rm em}$, as

$$I_{\rm em} \equiv \mu^{-2} \sum_{n_{\rm q=0}} \sum_{n_{\rm q=\pi}} \sum_{n_{\rm s,G}} |\langle \Psi_{\rm em} | \hat{\mu} | \Psi_{G,n_{\rm q=0},n_{\rm q=\pi},n_{\rm s,G}} \rangle|^2$$
(26)

Defined as such, $I_{\rm em}=1$ for noninteracting chromophores. A conventional H-dimer takes on values in the range $0 \le I_{\rm em} < 1$, while in a J-dimer, $1 < I_{\rm em} \le 2$. Maximal superradiance requires $I_{\rm em}=2$; however, the ratio $\gamma_{\rm D}/\gamma_{\rm M}$ is less than 2 in red-shifted PL because of the cubic transition frequency dependence in eqs 24 and 25. Note that the emission strength is proportional to the integrated area of the reduced PL spectrum, i.e.

$$I_{\rm em} = (\sqrt{2\pi} \,\sigma_{\rm H} \mu^2)^{-1} \int S(\omega) \,\mathrm{d}\omega \tag{27}$$

In what follows, we evaluate the absorption and PL spectra of dimers, beginning with the simplest case where only the slow mode is included, followed by the general case where both slow and fast modes are included. The monomer transition frequency is taken to be $E_{\rm M}=20{,}000~{\rm cm}^{-1}$, and for simplicity, we set D=0. (Increasing |D| to several hundred wave numbers will have negligible impact since $D\ll E_{\rm M}$.) To be as general as possible, we treat a broad range of $g_{\rm L}$ and $g_{\rm NL}$ values, realizing that all spectra are invariant to $(g_{\rm L},g_{\rm NL})\to$

 $(-g_{\rm L}, -g_{\rm NL})$. Finally, the fast mode is characterized by $\omega_{\rm f} = 1400~{\rm cm}^{-1}$ and $\lambda_{\rm f}^2 = 1$, while the slow-mode frequency is much smaller, $\omega_{\rm s} = 100~{\rm cm}^{-1}$.

3.1. Slow Mode Only. Figure 6a–d shows the T=0 K absorption and emission spectra for J- and H-dimers including only slow-mode vibronic coupling, as governed by the Hamiltonian in eq 10. For all spectra, the homogeneous line width $\sigma_{\rm H}$ (=40 cm⁻¹) is chosen to be small enough to resolve the slow-mode transitions. For the J-dimer in Figure 6a, the spectra are evaluated for a physically reasonable value of $g_{\rm NL}$ = +100 cm⁻¹ and for several $g_{\rm L}$ values, starting at –100 cm⁻¹ and increasing to +700 cm⁻¹. For the H-dimer in Figure 6b, $g_{\rm NL}$ = –100 cm⁻¹. The opposing signs of $g_{\rm NL}$ for H- and J-dimers and positive values for $g_{\rm L}$ are consistent with a slow stretching mode, as discussed earlier.

For both J- and H-dimers, the absorption spectrum is governed by the k=0 PES in Figure 3 and therefore depends only on $|g_{\rm NL}+g_{\rm L}|$; hence, we do not display the spectral series for a larger range of negative $g_{\rm L}$ values. As shown in Figure 6a,b, for both H- and J-dimers, the peak of the absorption spectrum appears at (or near) $E_{\rm M}+J_{\rm C}$. The spectrum is narrowest when the local and nonlocal couplings interfere destructively with $g_{\rm NL}+g_{\rm L}=0$. In this limit, the k=0 PES lies directly above the ground-state PES with no relative shift—see Figure 4a. Hence, the transition is entirely due to the 0–0 excitation with a line width of $2\sigma_{\rm H}$. As $|g_{\rm NL}+g_{\rm L}|$ increases, the k=0 well shifts relative to the ground-state well, causing the spectrum to substantially broaden as the 0-n transitions with n

> 0 begin to appear. When the shift is large enough, the Poisson distribution of 0-n intensities becomes approximately Gaussian. Identifying the slow-mode effective HR factor as $\lambda_s^2 = [(g_{\rm NL} + g_{\rm L})/2\omega_s]^2$, the evolution of the Poisson distribution to a normal distribution with increasing λs^2 is described as

$$e^{-\lambda_s^2} \frac{\lambda_s^{2n}}{n!} \to \frac{1}{\sqrt{2\pi\lambda_s^2}} e^{-(n-\lambda_s^2)^2/2\lambda_s^2}$$
 (28)

In this limit, the overall line width can be represented by the standard deviation

$$\sigma = \sqrt{\left(\frac{g_{\rm L} + g_{\rm NL}}{2}\right)^2 + \sigma_{\rm H}^2} \tag{29}$$

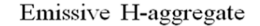
which accurately describes the broadening observed in Figure 6a,b. Interestingly, the peak absorption frequency is essentially constant, independent of $|g_{NL} + g_L|$. The peak absorption frequency is determined by the *vertical* transition energy, from the ground to the k = 0 PES, in accordance with the Franck—Condon principle (see blue arrow in Figures 3 and 4).

The k=0 PES is also responsible for PL in the J-dimer. The PL spectrum in Figure 6c significantly red-shifts and broadens with increasing $|g_{\rm NL}+g_{\rm L}|$, similar to what occurs in excimers. This is because, as in excimers, emission derives from the relaxed excited state. The magnitude of the Stokes red shift agrees well with the expression, $|J_{\rm C}| + \frac{(g_{\rm L}+g_{\rm NL})^2}{2\omega_{\rm s}}$, deduced from the level diagram in Figure 3. The broadening of the PL spectrum with increasing $|g_{\rm NL}+g_{\rm L}|$ is also well described by σ in eq 29.

Closer analysis shows that the integrated area of the reduced PL spectrum in Figure 6c for the J-dimer remains constant, independent of $g_{\rm L}$ and $g_{\rm NL}$, with the emission strength, $I_{\rm em}$, from eq 26 equal to its maximum value of 2. This means that if the cubic frequency factors in γ_D and γ_M in eqs 24 and 25 are neglected (equivalent to the limit of taking $E_{\rm M}$ to be very large), the radiative rate of the dimer would be exactly twice that of the monomer. The inset of Figure 6c shows that γ_D/γ_M \approx 1.85 when there is no local or nonlocal coupling, which is exactly equivalent to the spectra when $g_{\rm NL}$ + $g_{\rm L}$ = 0. The reduction of γ_D/γ_M below 2 is due entirely to the 500 cm $^{-1}$ red shift in the dimer versus monomer emission. Figure 6c also shows that $\gamma_{\rm D}/\gamma_{\rm M}$ diminishes as the PL red-shifts and is only slightly greater than unity when $g_{NL} + g_L$ reaches 800 cm⁻¹. Interestingly, all of the J-dimers in Figure 6c are superradiant $(\gamma_{\rm D}/\gamma_{\rm M}>1)$ despite the excimer-like appearance of the PL spectral line shape. Note that because g_L and g_{NL} remain inphase in Figure 6c, there is no possibility for the nonemissive Jaggregate discussed in Figure 5a.

In marked contrast to the J-dimer, there is no emission at all for the H-dimer when T=0 K. In the H-dimer, the lowest-energy PES has $k=\pi$. In line with the Kasha theory, $^{51-53}$ the emission is symmetry-forbidden. The presence of the symmetric slow-mode vibrations maintains the forbidden nature of the transition. Figure S.1 shows that the H-dimer can weakly emit if the higher-energy k=0 well is excited thermally, which occurs if the interwell separation is on the order of $k_{\rm b}T$. The figure also shows the additional broadening of both the absorption and PL spectra with increasing temperature.

Finally, we show in Figure 7 the absorption and PL spectra corresponding to the highly unusual superemissive H-dimer for



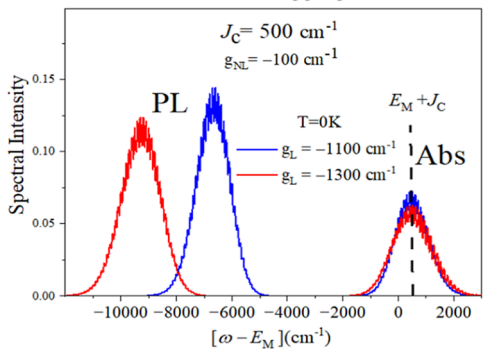


Figure 7. Calculated absorption and PL spectra for H-dimers with $J=500~{\rm cm^{-1}}$ and $g_{\rm NL}=-100~{\rm cm^{-1}}$ from eqs 21 and 23 based on the Hamiltonian in eq 10 with $\omega_{\rm s}=100~{\rm cm^{-1}}$. Spectra are shown for several values of local coupling, $g_{\rm L}$. Fast-mode EV coupling is neglected. In order to resolve the slow-mode vibronic structure, the homogeneous line width is set to $\sigma_{\rm H}=40~{\rm cm^{-1}}$.

in-phase values of g_L and g_{NL} which satisfy eq 14b. Absorption is blue-shifted relative to the monomer, as is characteristic of H-aggregates. However, emission is now strongly allowed since the k=0 PES is shifted below the $k=\pi$ PES, as depicted in Figure 5b. Moreover, the PL spectrum is strongly red-shifted as it is derived from the relaxed (k=0) PES. The peak of the PL spectrum occurs at

$$E_{\rm M} + J_{\rm C} - (g_{\rm NL} + g_{\rm L})^2 / 2\omega_{\rm s}$$

which is readily deduced from Figure 3. Interestingly, the emission strength, $I_{\rm em}$, from eq 26 is exactly 2, as for the J-dimers in Figure 6c. Such unusual H-dimers are referred to as superemissive, even though $\gamma_{\rm D}/\gamma_{\rm M}$ can drop below unity due to the large PL red shift. (Note that such unusual behavior cannot be induced by a slow *stretching* mode since $g_{\rm NL}$ and $g_{\rm L}$ are out-of-phase.)

3.2. Fast and Slow Modes. We now incorporate both fast and slow vibrations through the FHP Hamiltonian in eq 1. The fast-mode energy is taken to be $\omega_{\rm f}=1400~{\rm cm}^{-1}$, as is typical for a vinyl stretching mode and therefore much greater than the slow-mode energy. The HR factor, $\lambda_{\rm f}^2$, is taken to be unity $(\lambda_{\rm f}^2=1)$ such that the first two vibronic peaks, A_1 and A_2 , in the vibronic progression characterizing the absorption spectrum of the monomer are equal, as depicted in Figure 8. The 0–0 and 0–1 vibronic peaks in the (reduced) PL spectrum of the monomer are also equal when the HR factor is unity.

Figure 9 shows the absorption and PL spectra for J- and H-dimers based on the chromophore in Figure 8, with J_C and $g_{\rm NL}$ being identical to the values of Figure 6 and for a range of positive $g_{\rm L}$ values. Figure 10 shows the negative $g_{\rm L}$ values. In both figures, we have increased the homogeneous line width to $\sigma_{\rm H}=400~{\rm cm}^{-1}$, in order to simplify the spectra so that only the fast-mode structure is observed. The vibronic progression ($A_{\rm I}$, $A_{\rm 2}$, ...) in the absorption spectra is clearly discerned but with vibronic intensities which differ substantially from those in the monomer of Figure 8. Figures 9a and 9b (as well as Figure 10a,b) clearly show an enhancement and reduction, respectively, of the $A_{\rm I}/A_{\rm 2}$ intensity ratio, consistent with what has been established for J- and H-aggregates in the absence of slow-mode coupling. 23,24 Figure 11 shows that the $A_{\rm I}/A_{\rm 2}$ ratio, evaluated from the spectral area of each peak, is independent of slow-mode coupling. The ratio is practically

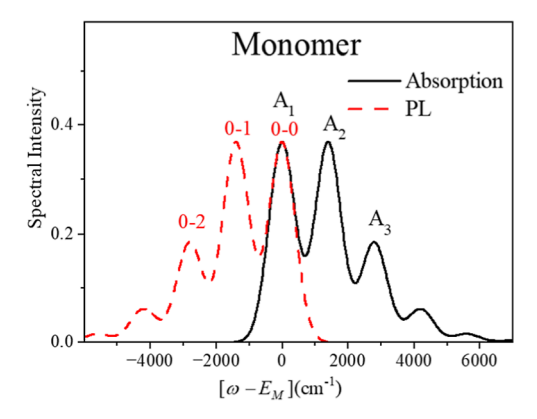


Figure 8. Absorption spectrum and (reduced) PL spectrum for a monomer showing vibronic progression with mode energy of 1400 cm⁻¹ and HR factor $\lambda_{\rm f}^2=1$. The line width is $\sigma_{\rm H}=400~{\rm cm}^{-1}$.

identical to that obtained when there is no slow-mode coupling at all, $g_{\rm NL} = g_{\rm L} = 0$, as shown in Figure S.2. The above analysis shows that the A_1/A_2 ratio can be computed using the perturbative expressions derived earlier in the absence of the slow-mode coupling.^{23,24}

The PL spectra in Figures 9c,d and 10c,d are more complex. For the J-dimer, the PL spectra in Figures 9c and 10c also display a clear fast-mode vibronic progression, dominated by the 0-0 peak. In the absence of the slow-mode coupling, the 0-0/0-1 ratio for the reduced PL spectrum in a disorder-free

J-aggregate (at 0 K) containing N chromophores was shown to abide by $^{2.5}$

$$I_{0-0}/I_{0-1} = N/\lambda_f^2 \tag{30}$$

which is exactly 2 for the dimer (N=2) in Figure 9 with $\lambda_{\rm f}^2=1$. Figure 9c shows that the PL ratio rule also holds in the presence of local and nonlocal couplings to the slow mode. Although the line width increases substantially with increasing $g_{\rm L}+g_{\rm NL}$, the 0-0/0-1 ratio remains steadfast at the value of 2 (after accounting for the effect of overlapping peaks). An exception is the subradiant J-aggregate in Figure 10c which occurs for sufficiently large and out-of-phase $g_{\rm L}$ and $g_{\rm NL}$ values (see eq 14a). The PL spectrum lacks the 0-0 peak entirely (although difficult to appreciate from the figure due to excessive line broadening). Figure S.2 further shows the dependence of the entire spectrum on particular values of $g_{\rm L}$ and $g_{\rm NL}$ in the limit that the sum is zero.

As shown in Figures 9d and 10d, photoluminescence for the H-dimer is no longer forbidden at T=0 K when the fast mode is activated. This result is well-known^{23,24} in the absence of slow-mode coupling. For the H-dimer, PL is made possible by the last term in the Hamiltonian in eq 15 which allows for coupling between states in the k=0 well and states in the $k=\pi$ well, as long as the overall state symmetries are the same, as in the case of Herzberg–Teller (HT) coupling. Hence, the $k=\pi$ lowest-energy exciton with no fast-mode vibrational quanta can mix with the higher energy k=0 exciton with a single quantum of the fast-mode antisymmetric $(q=\pi)$ vibrational mode; see eq 19. Subsequent emission is symmetry-allowed if

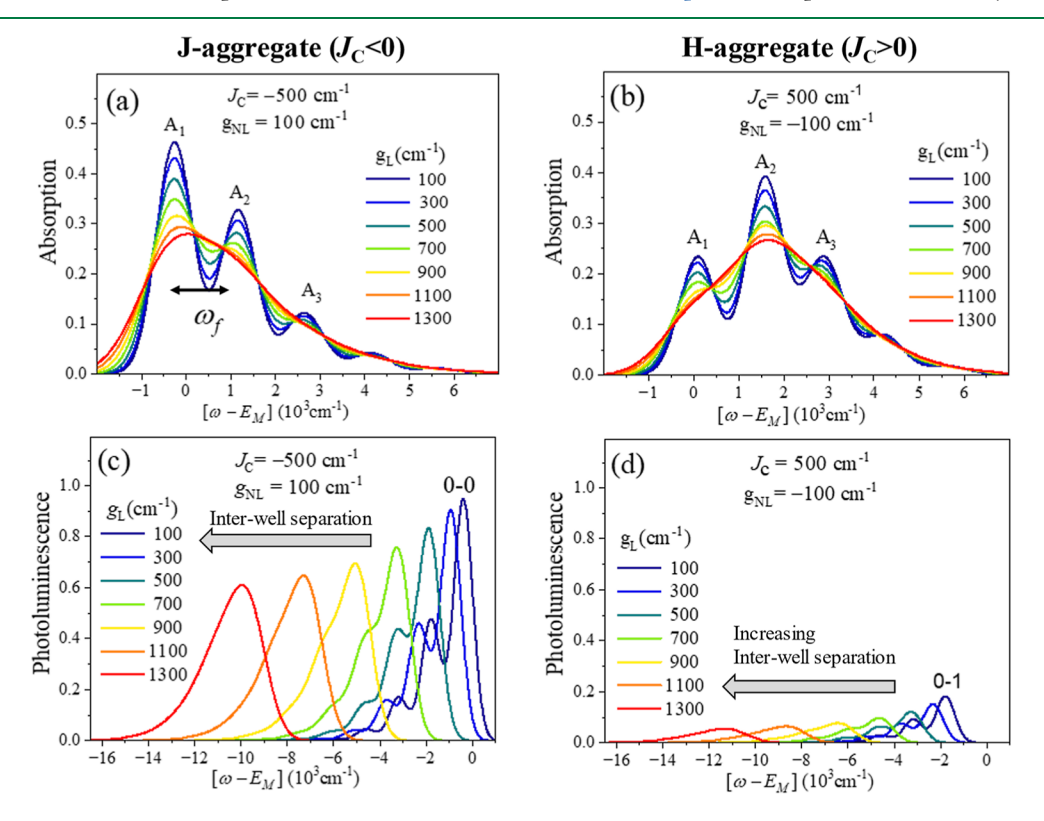


Figure 9. Absorption and (reduced) PL spectra at T=0 K for J-dimers (left) and H-dimers (right) evaluated from eqs 21 and 23 based on the $H_{\rm FHP}$ Hamiltonian in eq 15. Spectra are shown for a range of $g_{\rm L}$ (>0) values, with $g_{\rm NL}$ held constant at 100 cm⁻¹ in the J-dimer and -100 cm⁻¹ in the H-dimer, with the sign consistent with a symmetric stretch; see text. In all cases, the interwell separation increases with $g_{\rm L}$ as indicated by the gray arrows. This requires $g_{\rm NL}g_{\rm L}$ to be in-phase for J-dimers and out-of-phase for H-dimers (see eq 13a and 13b). The reduced PL spectrum is evaluated without the cubic transition frequency term. In all cases, $\omega_s=100$ cm⁻¹, and the fast mode is parametrized using $\omega_f=1400$ cm⁻¹ and $\lambda_f^2=1$. The homogeneous line width is $\sigma_{\rm H}=400$ cm⁻¹.

ı

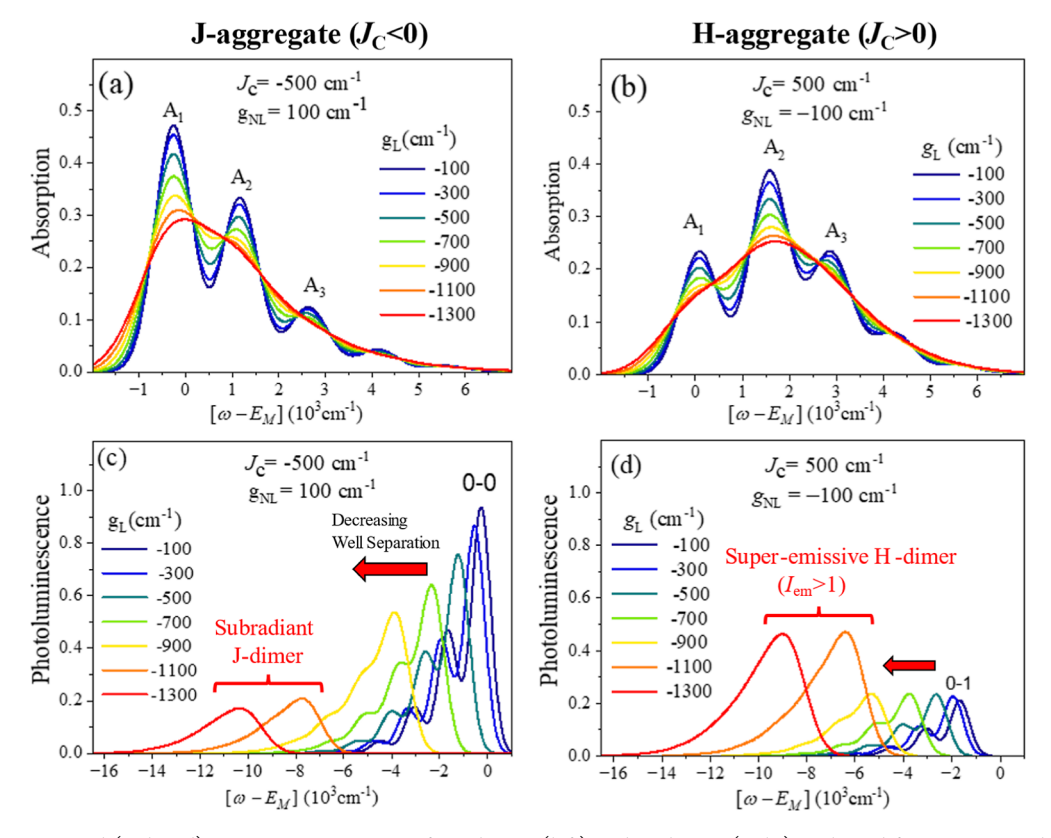


Figure 10. Absorption and (reduced) PL spectra at T=0 K for J-dimers (left) and H-dimers (right) evaluated from eqs 21 and 23 based on the H_{FHP} Hamiltonian in eq 15. Spectra are shown for a range of g_L (< 0) values, with g_{NL} held constant at 100 cm⁻¹ in the J-dimer and -100 cm⁻¹ in the H-dimer, with the sign consistent with a symmetric stretch; see text. In all cases, the interwell separation decreases with increasing $|g_L|$ as indicated by the red arrows, until the two wells become degenerate when $g_L = -1000$ cm⁻¹. This requires $g_{NL}g_L$ to be out-of-phase for J-dimers and in-phase for H-dimers (see eqs 13a and 13b). The reduced PL spectrum is evaluated without the cubic transition frequency term. In all cases, $ω_s = 100$ cm⁻¹, and the fast mode is parametrized using $ω_f = 1400$ cm⁻¹ and $λ_f^2 = 1$. The homogeneous line width is $σ_H = 400$ cm⁻¹.

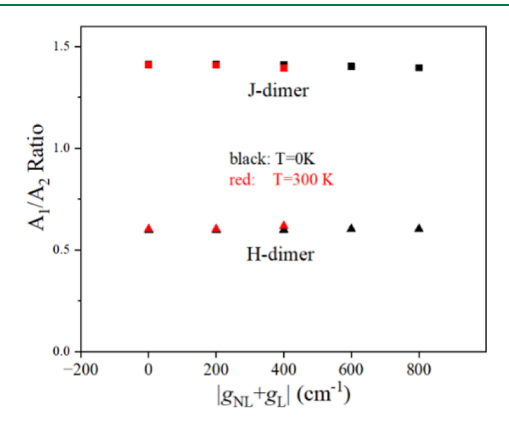


Figure 11. Absorption spectral ratio A_1/A_2 from Figures 9 and 10 as a function of $|g_L + g_{\rm NL}|$.

it terminates on the ground state containing a single antisymmetric fast-mode $(q = \pi)$ vibration, i.e., 0-1 emission. A more general analysis shows that PL emission from an ideal H-aggregate (no disorder, T = 0 K) is entirely devoid of 0-0 emission but generally contains satellite emission (0-1, 0-2, ...). When slow-mode coupling is activated, the 0-0 emission remains forbidden since the slow mode is fully symmetric. This is clear from Figure 9d, which further shows that increased slow-mode coupling causes increased line broadening and increased red-shifting. Importantly, the PL intensity in Figure 9d is greatly diminished relative to the J-dimer in Figure 9c. The conventional H-aggregate emission is

subradiant; a glaring exception is the highly unusual superemissive H-aggregate shown in Figure 10d which results from the energetic reversal of the k=0 and π wells (see Figure 5b) for sufficiently large and in-phase $g_{\rm L}$ and $g_{\rm NL}$ values (see eq 14b). Spectra at T=300 K are shown in Figure S.3.

3.3. Slow-Mode Impact on the Radiative Decay Rate. With the fast mode present, activating EV coupling to the slow mode can diminish *or enhance* the radiative decay rate in J- and H-dimers, depending on the sign of the product g_Lg_{NL} . The latter impacts the interwell energy gap $(\Delta_J \text{ or } \Delta_H)$ according to eqs 13a and 13b, which, in turn, affects the interwell Herzberg—Teller (HT) coupling induced by the presence of the fast mode, as represented by the last term in the Hamiltonian in eq 15. For a J-dimer, an increase in Δ_J lessens the HT-induced mixing of the emissive k=0 state with the higher-energy nonemissive $k=\pi$ states, leading to an *enhanced* radiative rate. For H-dimers, an increase in Δ_H lessens the HT-induced mixing between the nonemissive $k=\pi$ state and the higher-energy emissive k=0 states, leading to an *attenuated* radiative decay rate.

We consider first the J-dimer. When the slow-mode coupling is neglected entirely, the radiative decay rate $\gamma_{\rm D}$ from eq 24 is calculated to be about $1.85\gamma_{\rm M}-$ –almost fully superradiant. Figure 12a shows the effect of increasing $g_{\rm L}$ on $\gamma_{\rm D}/\gamma_{\rm M}$ and $I_{\rm em}$ while holding $g_{\rm NL}$ at $100~{\rm cm}^{-1}$ (as in Figures 9c and 10c). For a J-dimer, increasing the product $g_{\rm L}g_{\rm NL}$ increases the interwell separation, $\Delta_{\rm J}$, as indicated by the black solid arrow. The vertical dash line in Figure 12a indicates the value at which $\Delta_{\rm I}$

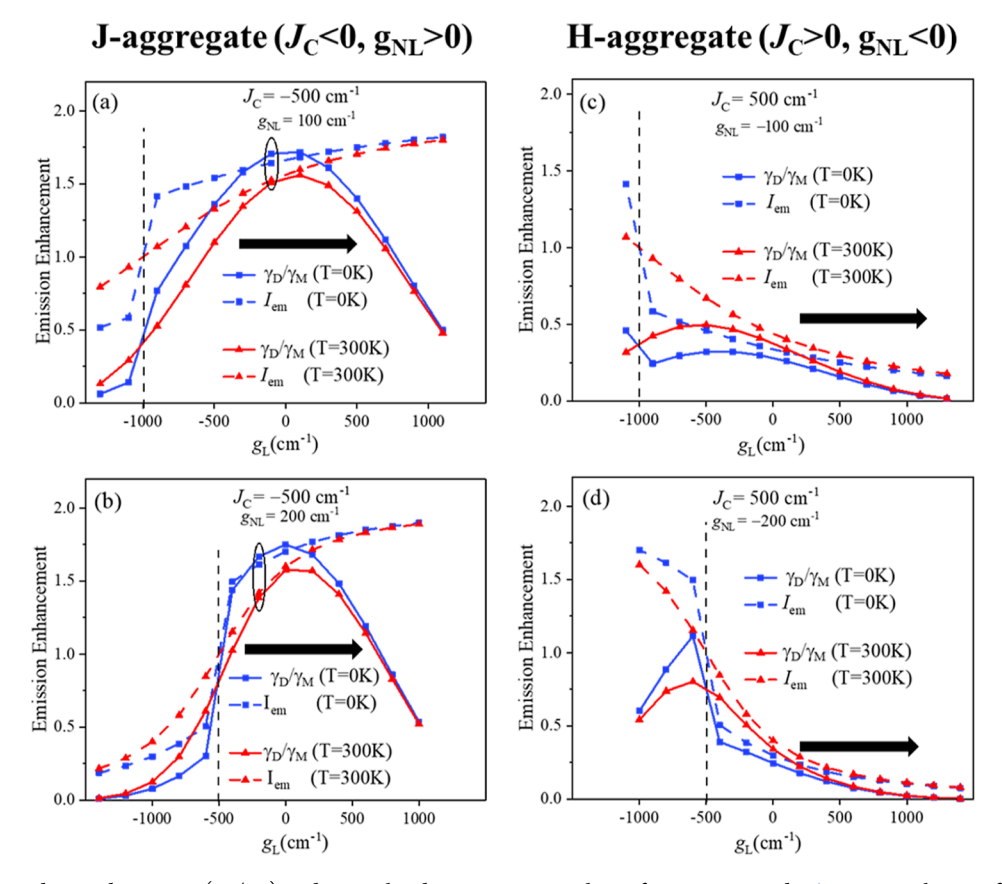


Figure 12. Relative radiative decay rate (γ_D/γ_M) and normalized emission strength $I_{\rm em}$ from eqs 24 and 26, respectively, as a function of $g_{\rm L}$ for J-dimers (left) and H-dimers (right) based on the $H_{\rm FHP}$ Hamiltonian in eq 15. For the J-dimer, $g_{\rm NL}$ is held constant at 100 cm⁻¹ in (a) and 200 cm⁻¹ in (b). The values are negated for the H-dimer in (c,d). Blue (red) curves correspond to T=0 K (T=300 K). The interwell separation increases in the direction indicated with the black arrow. The vertical dash line indicates the point at which the interwell separation is zero—i.e., degenerate k=0 and $k=\pi$ wells. Encircled points indicate $g_{\rm NL}+g_{\rm L}=0$. In all cases, $\omega_s=100$ cm⁻¹, D=0, $\omega_{\rm f}=1400$ cm⁻¹, and $\lambda_{\rm f}^2=1$.

is zero; below this value, one has the unusual subradiant Jaggregate discussed earlier, where the $k = \pi$ well drops below the k = 0 well. Increasing g_L beyond the vertical line leads to a steady increase in the emission strength, I_{em} (dashed curves), as well as $\gamma_{\rm D}/\gamma_{\rm M}$ (solid curves) due to the resulting HTdecoupling of the two wells. When $g_L + g_{NL} = 0$ (indicated by the oval), γ_D/γ_M is approximately 1.75 at T=0 K and slightly lower at 300 K. These values are essentially equal to those obtained when there is no slow-mode coupling at all (see Figure S.2). Surprisingly, γ_D slightly increases with $g_L + g_{NL}$ beyond this value (especially at 300 K) before peaking and then diminishing. The latter is due to the cubic frequency dependence on γ_D and the strong red-shifting of the PL spectrum, as shown in Figure 9c. Note that I_{em} , which lacks the cubic frequency dependence, maintains a monotonic increase with $g_L + g_{NL}$, eventually converging to the maximum value of $I_{\rm em}$ = 2, indicative of uncoupled wells. Figure 12b shows the effect of increasing $g_{\rm NL}$ to 200 cm⁻¹. The increase in superradiance with g_L + g_{NL} beyond zero is even more pronounced. The increase in superradiance induced by slowmode coupling is quite unusual, as nuclear motion is intuitively expected to disrupt the superradiance.

For the H-dimer, the situation is reversed. As captured in Figure 12c,d both $\gamma_{\rm D}/\gamma_{\rm M}$ and $I_{\rm em}$ initially decrease as $g_{\rm L}$ increases beyond the vertical line. This is associated with an increase in the interwell separation, $\Delta_{\rm H}$, which reduces the HT coupling required to make emission symmetry-allowed from the $k=\pi$ well. Hence, slow-mode coupling leads to enhanced

subradiance relative to the case with no slow-mode coupling. The figure also shows that below the vertical line—when the k=0 well is energetically shifted below the $k=\pi$ well——the radiation rate dramatically increases, with $\gamma_{\rm D}/\gamma_{\rm M}$ becoming a substantial fraction of the monomer rate and even superradiant.

Before concluding, we briefly discuss the important limiting case, $g_{\rm L}g_{\rm NL}=0$. In this limit, there is no change in the interwell gap; both $\Delta_{\rm J}$ and $\Delta_{\rm H}$ remain equal to the exciton bandwidth 2l $J_{\rm C}$ l. When only local coupling to the slow mode is active (i.e., $g_{\rm L}\neq 0$, $g_{\rm NL}=0$), analysis of the emission strength $I_{\rm em}$ from eq 26 shows that it does not change at all with $g_{\rm L}$. In this case, both wells are shifted in the same direction with equal relaxation energies. Hence, the HT coupling between wells is unchanged. However, when only nonlocal coupling is operative (i.e., $g_{\rm NL}\neq 0$, $g_{\rm L}=0$), there is a substantial change in the horizontal interwell separation, since the wells are shifted in opposite directions (see Figure 3). This also induces interwell HT decoupling for large values of $g_{\rm NL}>400~{\rm cm}^{-1}$, as shown in Figure S.4. In this case, $I_{\rm em}$ increases (decreases) with $|g_{\rm NL}|$ in J-dimers (H-dimers).

4. DISCUSSION/CONCLUSIONS

Utilizing a Frenkel-Holstein-Peierls Hamiltonian, a fully quantum-mechanical analysis of absorption and emission in H-and J-dimers is presented, incorporating both local and nonlocal EV coupling to a slow intermolecular vibration (i.e., lattice phonon) as well as local coupling to the fast vinyl-

stretching intramolecular mode. The latter is responsible for pronounced vibronic progressions observed in many organic chromophores with mode energies of approximately 1400 cm⁻¹. Generally, both local and nonlocal slow-mode coupling lead to spectral broadening and red-shifted emission spectra for J- and H-dimers, as is characteristic of self-trapped excitons and excimers. For a slow mode which preserves symmetry, such as a simple intermolecular stretching mode, it is found that the vibronic ratio rules²³⁻²⁵ for describing J- and H-aggregation, remain valid in the presence of both local and nonlocal coupling. Since the vibronic peak ratio A_1/A_2 responds directly to the free-exciton bandwidth $2|J_C|$, the insensitivity to slowmode coupling is at first surprising, since nonlocal coupling alters the Coulomb coupling. However, absorption is a vertical FC excitation process which is sensitive to the Coulomb coupling, J_C , corresponding to the ground-state geometry. In contrast, the 0-0/0-1 PL ratio responds directly to the exciton coherence number, which, for the dimer, remains at the value of 2 since the slow mode preserves symmetry. Hence, in the conventional J-dimer, the 0-0/0-1 ratio remains independent of g_L and g_{NL} , as seen in Figure 9c. By marked contrast, in the H-dimer, the 0-0 peak remains absent (at T =0 K). In larger aggregates, the presence of nontotally symmetric lattice phonons will of course impact the spectral ratios, but in the adiabatic limit, slow-mode coupling can be treated as a temperature-dependent site disorder, ^{59,60°} and the ratio rules already derived for static inhomogeneous disorder^{23–25} should be applicable for understanding general lattice-phonon couplings.

Generally, we find that the absorption and emission spectra respond to an interference between local and nonlocal couplings. As demonstrated in Figure 3, in the presence of slow-mode coupling alone, the k = 0 and $k = \pi$ wells shift along q_s by $-(g_{\rm NL}+g_{\rm L})/2\omega_{\rm s}$ and $(g_{\rm NL}-g_{\rm L})/2\omega_{\rm s}$, respectively, with the corresponding relaxation energies $(g_L + g_{NL})^2/4\omega_s$ and $(g_L$ $-g_{\rm NL})^2/4\omega_{\rm s}$ Interference effects are manifest in the absorption and PL spectral line widths as well as the PL red-shifts, as summarized for J- and H-dimers in Figures 6, 9, and 10. Interestingly, in the case of J-dimers, superradiance remains operative as the PL increasingly red-shifts, as shown in Figure 12a,b, where the radiative decay rate exceeds the monomer value for substantial values of $|g_{NL} + g_L|$. Excimer-like emission has been reported in J-aggregates of thiaminomethinecyanine dyes⁶¹ and attributed to energy migration to dimer-trapping sites. There are also several works involving J-aggregates, where the PL spectrum includes a broad, red-shifted component which was attributed to exciton self-trapping due to local slow-mode coupling. It would be interesting to see if nonlocal coupling plays a role in such cases.

Perhaps the most striking impact of the local/nonlocal slow-mode coupling is its ability to alter the coupling between the k=0 and $k=\pi$ potential energy wells caused by fast-mode EV coupling (the last term in eq 15). Whenever the product g_Lg_{NL} is positive (negative), the energetic separation between the wells initially *decreases* in H-dimers (J-dimers), as indicated in Figure 3, leading to enhanced interwell coupling. For H-dimers, bringing the two wells closer together enables more efficient HT coupling, which increases the emission transition dipole and radiative decay rate. For J-dimers, more efficient coupling has the opposite effect. The overall behavior is summarized in Figure 12. Perhaps most surprisingly, the emission strength, $I_{\rm em}$, in J-dimers ($g_{\rm NL}>0$) increases as the total coupling $g_{\rm NL}+g_L$ increases beyond zero, as observed in

Figure 12a,b—i.e., superradiance can be induced by slow-mode coupling. The coupling between the k=0 and $k=\pi$ wells also depends on their relative *horizontal* shift. For example, when only $g_{\rm NL}$ is present ($g_{\rm L}=0$) the vertical shift remains at $2|J_{\rm C}|$, independent of $g_{\rm NL}$. Increasing $|g_{\rm NL}|$ leads to an increasing horizontal separation between the oppositely-shifted wells, leading to inter-well decoupling and changes to the emission enhancement, as shown in Figure S.2. Generally, the interwell coupling depends very much on the particular form of the intermolecular mode from which $g_{\rm L}$ and $g_{\rm NL}$ are derived. In this work, we considered a simple stretching mode; other modes, such as torsional modes and shearing modes, will be explored in future works. We also expect similar interwell coupling effects to exist in more physically realistic anharmonic wells or between harmonic wells of different curvatures.

In the extreme case where the product $g_L g_{NL}$ exceeds $2J_C \omega_s$ in an H-dimer $(I_C > 0)$, the k = 0 well relaxes below the $k = \pi$ well (see Figure 5b) leading to highly unconventional strongly emissive or even superradiant H-dimers, despite a large PL redshift and broadening. For the J-dimer ($J_C < 0$), the conversion to a subradiant J-dimer, portrayed in Figure 5a, occurs when $g_L g_{NL} < 2J_C \omega_s$. (Note that unlike for the emissive H-dimer, g_L and g_{NL} must now have opposite signs since J_C is negative.) Emission is characterized by a broad, red-shifted PL spectrum, quite similar to that of an excimer. Such dramatic effects do, however, require sizeable local and nonlocal couplings, which are easier to physically justify when Frenkel-CT mixing is included in a more generalized Hamiltonian. This can be accomplished by replacing J_C in the Frenkel Hamiltonian in eq 2 with $J_{\rm C}$ + $J_{\rm CT}$ and D by D + $\Delta_{\rm CT}$. Here, $J_{\rm CT}$ and $\Delta_{\rm CT}$ are derived from a perturbative treatment of Frenkel-CT mixing, as is justified in the limit of well-separated (diabatic) Frenkel and CT bands. 23,55 The local and nonlocal coupling parameters are then determined from $d(D + \Delta_{CT})/dq_s$ and $d(J_C + J_{CT})/dq_s$, respectively, which are expected to be quite large due to the strong sensitivity of Δ_{CT} and J_{CT} to small displacements in the relative positions of neighboring chromophores.⁵⁶ For the more general case where the diabatic Frenkel and CT bands are closer in energy, one must expand the basis set to include CT states as was done in ref 44.

Finally, the present work needs to be extended to one-dimensional aggregates in order to determine how the interference between local and nonlocal couplings impacts the photophysical response as well as energy transport. The inclusion of nontotally symmetric lattice modes which accompany a larger aggregate with N>2 leads to a more complex picture, as shown by several recent works which considered the impact of EV coupling on coherent energy transfer in molecular trimers. ^{19,21} In larger systems, the effect of local and nonlocal coupling on exciton self-trapping ⁷ and transport, ^{6,14} as well as charge transport, ⁴⁵ has also been addressed, but the impact on the photophysical response has not received as much attention. In future works, we plan to focus primarily on the spectral signatures of exciton self-trapping due to local and nonlocal coupling in larger systems.

ASSOCIATED CONTENT

Supporting Information

The Supporting Information is available free of charge at https://pubs.acs.org/doi/10.1021/acs.jctc.4c00299.

Expressions for absorption and PL with thermal averaging, room-temperature H- and J-dimer spectra

including coupling to just the slow mode as well as coupling to both fast and slow modes, spectra for $g_L + g_{NL} = 0$, and an analysis of the impact of just nonlocal coupling on the radiative decay rates in H- and J-dimers (PDF)

AUTHOR INFORMATION

Corresponding Author

Frank C. Spano — Department of Chemistry, Temple University, Philadelphia, Pennsylvania 19122, United States; orcid.org/0000-0003-3044-6727; Email: spano@temple.edu

Author

Hamed Haghshenas — Department of Chemistry, Temple University, Philadelphia, Pennsylvania 19122, United States; orcid.org/0000-0003-2056-7584

Complete contact information is available at: https://pubs.acs.org/10.1021/acs.jctc.4c00299

Notes

The authors declare no competing financial interest.

ACKNOWLEDGMENTS

This work was performed under the financial support for F.C.S. from the National Science Foundation (DMR-2221923).

REFERENCES

- (1) Toyozawa, Y. Optical Processes in Solids; Cambridge University Press, 2003.
- (2) Levinson, Y. B.; Rashba, E. I. Electron-phonon and exciton-phonon bound states. *Rep. Prog. Phys.* **1973**, *36*, 1499–1565.
- (3) Rashba, E. I.; Sturge, M. D. *Excitons*; North-Holland Publishing Company, 1982.
- (4) Sumi, H.; Sumi, A. Dimensionality dependence in self-trapping of excitons. *J. Phys. Soc. Jpn.* **1994**, *63*, *637*–*657*.
- (5) Higai, S. i.; Sumi, H. Two types of self-trapped states for excitons in one dimension. *J. Phys. Soc. Jpn.* **1994**, *63*, 4489–4498.
- (6) Munn, R. W.; Silbey, R. Theory of electronic transport in molecular crystals. Ii. Zeroth order states incorporating nonlocal linear electron—phonon coupling. *J. Chem. Phys.* **1985**, *83*, 1843—1853.
- (7) Zhao, Y.; Brown, D. W.; Lindenberg, K. A variational approach to nonlocal exciton—phonon coupling. *J. Chem. Phys.* **1997**, *106*, 2728–2740.
- (8) Brixner, T.; Hildner, R.; Köhler, J.; Lambert, C.; Würthner, F. Exciton transport in molecular aggregates from natural antennas to synthetic chromophore systems. *Adv. Energy Mater.* **2017**, *7*, 1700236.
- (9) Sneyd, A. J.; Fukui, T.; Paleček, D.; Prodhan, S.; Wagner, I.; Zhang, Y.; Sung, J.; Collins, S. M.; Slater, T. J. A.; Andaji-Garmaroudi, Z.; et al. Efficient energy transport in an organic semiconductor mediated by transient exciton delocalization. *Sci. Adv.* **2021**, *7*, No. eabh4232.
- (10) Alvertis, A. M.; Pandya, R.; Muscarella, L. A.; Sawhney, N.; Nguyen, M.; Ehrler, B.; Rao, A.; Friend, R. H.; Chin, A. W.; Monserrat, B. Impact of exciton delocalization on exciton-vibration interactions in organic semiconductors. *Phys. Rev. B* **2020**, *102*, 081122.
- (11) Nelson, T. R.; Ondarse-Alvarez, D.; Oldani, N.; Rodriguez-Hernandez, B.; Alfonso-Hernandez, L.; Galindo, J. F.; Kleiman, V. D.; Fernandez-Alberti, S.; Roitberg, A. E.; Tretiak, S. Coherent exciton-vibrational dynamics and energy transfer in conjugated organics. *Nat. Commun.* **2018**, *9*, 2316.
- (12) Aragó, J.; Troisi, A. Dynamics of the excitonic coupling in organic crystals. *Phys. Rev. Lett.* **2015**, *114*, 026402.

- (13) Aragó, J.; Troisi, A. Regimes of exciton transport in molecular crystals in the presence of dynamic disorder. *Adv. Funct. Mater.* **2016**, 26, 2316–2325.
- (14) Jiang, L.; Hirst, J. D.; Do, H. Dynamic disorder drives exciton dynamics in diketopyrrolopyrrole—thiophene-containing molecular crystals. *J. Phys. Chem. C* **2023**, *127*, 5519—5532.
- (15) Binder, R.; Polkehn, M.; Ma, T. J.; Burghardt, I. Ultrafast exciton migration in an hj-aggregate: Potential surfaces and quantum dynamics. *Chem. Phys.* **2017**, 482, 16–26.
- (16) Mondelo-Martell, M.; Brey, D.; Burghardt, I. Quantum dynamical study of inter-chain exciton transport in a regioregular p3ht model system at finite temperature: Hj vs h-aggregate models. *J. Chem. Phys.* **2022**, *157*, 094108.
- (17) Barford, W. Exciton dynamics in conjugated polymer systems. *Front. Phys.* **2022**, *10*, 1004042.
- (18) Jang, S. J. Effects of donor—acceptor quantum coherence and non-markovian bath on the distance dependence of resonance energy transfer. *J. Phys. Chem. C* **2019**, *123*, *5767*–*5775*.
- (19) Cina, J. A. Dynamics of an excitation-transfer trimer: Interference, coherence, berry's phase development, and vibrational control of non-adiabaticity. *J. Chem. Phys.* **2023**, *158*, 124307.
- (20) Biggs, J. D.; Cina, J. A. Studies of impulsive vibrational influence on ultrafast electronic excitation transfer. *J. Phys. Chem. A* **2012**, *116*, 1683–1693.
- (21) Makri, N. Electronic frustration, berry's phase interference and slow dynamics in some tight-binding systems coupled to harmonic baths. *J. Phys. A: Math. Theor.* **2023**, *56*, 144001.
- (22) Barford, W.; Marcus, M. Perspective: Optical spectroscopy in π -conjugated polymers and how it can be used to determine multiscale polymer structures. *J. Chem. Phys.* **2017**, *146*, 130902.
- (23) Hestand, N. J.; Spano, F. C. Expanded theory of h- and j-molecular aggregates: The effects of vibronic coupling and intermolecular charge transfer. *Chem. Rev.* **2018**, *118*, 7069–7163.
- (24) Spano, F. C. The spectral signatures of frenkel polarons in hand j-aggregates. Acc. Chem. Res. 2010, 43, 429-439.
- (25) Spano, F. C.; Yamagata, H. Vibronic coupling in j-aggregates and beyond: A direct means of determining the exciton coherence length from the photoluminescence spectrum. *J. Phys. Chem. B* **2011**, *115*, 5133–5143.
- (26) Eisfeld, A.; Briggs, J. S. The j- and h-bands of organic dye aggregates. *Chem. Phys.* **2006**, 324, 376–384.
- (27) Bloemsma, E. A.; Silvis, M. H.; Stradomska, A.; Knoester, J. Vibronic effects and destruction of exciton coherence in optical spectra of j-aggregates: A variational polaron transformation approach. *Chem. Phys.* **2016**, *481*, 250–261.
- (28) Halpin, A.; Johnson, P. J. M.; Tempelaar, R.; Murphy, R. S.; Knoester, J.; Jansen, T. L. C.; Miller, R. J. D. Two-dimensional spectroscopy of a molecular dimer unveils the effects of vibronic coupling on exciton coherences. *Nat. Chem.* **2014**, *6*, 196–201.
- (29) Hestand, N. J.; Tempelaar, R.; Knoester, J.; Jansen, T. L. C.; Spano, F. C. Exciton mobility control through sub-angstrom packing modifications in molecular crystals. *Phys. Rev. B: Condens. Matter Mater. Phys.* **2015**, *91*, 195315.
- (30) Tempelaar, R.; Spano, F. C.; Knoester, J.; Jansen, T. L. C. Mapping the evolution of spatial exciton coherence through time-resolved fluorescence. *J. Phys. Chem. Lett.* **2014**, *5*, 1505–1510.
- (31) Kumar, S.; Dunn, I. S.; Deng, S. B.; Zhu, T.; Zhao, Q. C.; Williams, O. F.; Tempelaar, R.; Huang, L. B. Exciton annihilation in molecular aggregates suppressed through qu antum interference. *Nat. Chem.* **2023**, *15*, 1118–1126.
- (32) Malyukin, Y. V.; Sorokin, A. V.; Semynozhenko, V. P. Features of exciton dynamics in molecular nanoclusters (j-aggregates): Exciton self-trapping (review article). *Low Temp. Phys.* **2016**, *42*, 429–440.
- (33) Sorokin, A. V.; Ropakova, I. Y.; Wolter, S.; Lange, R.; Barke, I.; Speller, S.; Yefimova, S. L.; Malyukin, Y. V.; Lochbrunner, S. Exciton dynamics and self-trapping of carbocyanine j-aggregates in polymer films. J. Phys. Chem. C 2019, 123, 9428–9444.
- (34) Drobizhev, M.; Sapozhnikov, M.; Scheblykin, I.; Varnavsky, O.; Van der Auweraer, M.; Vitukhnovsky, A. Relaxation and trapping of

- excitons in j-aggregates of a thiacarbocynine dye. *Chem. Phys.* **1996**, 211, 455–468.
- (35) Sorokin, A. V.; Pereverzev, N. V.; Grankina, I. I.; Yefimova, S. L.; Malyukin, Y. V. Evidence of exciton self-trapping in pseudoisocyanine j-aggregates formed in layered polymer films. *J. Phys. Chem. C* **2015**, *119*, 27865–27873.
- (36) Katrich, G. S.; Kemnitz, K.; Malyukin, Y. V.; Ratner, A. M. Distinctive features of exciton self-trapping in quasi-one-dimensional molecular chains (j-aggregates). *J. Lumin.* **2000**, *90*, 55–71.
- (37) Malyukin, Y. Coexistence of free and self-trapped excitons in disordered j-aggregates. *Phys. Status Solidi C* **2006**, *3*, 3386–3393.
- (38) Young, R. M.; Wasielewski, M. R. Mixed electronic states in molecular dimers: Connecting singlet fission, excimer formation, and symmetry-breaking charge transfer. *Acc. Chem. Res.* **2020**, *53*, 1957–1968.
- (39) Bae, Y. J.; Shimizu, D.; Schultz, J. D.; Kang, G.; Zhou, J.; Schatz, G. C.; Osuka, A.; Wasielewski, M. R. Balancing charge transfer and frenkel exciton coupling leads to excimer formation in molecular dimers: Implications for singlet fission. *J. Phys. Chem. A* **2020**, *124*, 8478–8487.
- (40) Slifkin, M. A. Charge transfer and excimer formation. *Nature* **1963**, 200, 766–767.
- (41) Kim, W.; Nowak-Król, A.; Hong, Y.; Schlosser, F.; Würthner, F.; Kim, D. Solvent-modulated charge-transfer resonance enhancement in the excimer state of a bay-substituted perylene bisimide cyclophane. *J. Phys. Chem. Lett.* **2019**, *10*, 1919–1927.
- (42) Bialas, D.; Kirchner, E.; Röhr, M. I. S.; Würthner, F. Perspectives in dye chemistry: A rational approach toward functional materials by understanding the aggregate state. *J. Am. Chem. Soc.* **2021**, *143*, 4500–4518.
- (43) Hammer, S.; Linderl, T.; Tvingstedt, K.; Brütting, W.; Pflaum, J. Spectroscopic analysis of vibrational coupling in multi-molecular excited states. *Mater. Horiz.* **2023**, *10*, 221–234.
- (44) Bialas, A. L.; Spano, F. C. A holstein—peierls approach to excimer spectra: The evolution from vibronically structured to unstructured emission. *J. Phys. Chem. C* **2022**, *126*, 4067–4081.
- (45) Li, W.; Ren, J.; Shuai, Z. A general charge transport picture for organic semiconductors with nonlocal electron-phonon couplings. *Nat. Commun.* **2021**, *12*, 4260.
- (46) Coropceanu, V.; Cornil, J.; da Silva Filho, D. A.; Olivier, Y.; Silbey, R.; Bredas, J. L. Charge transport in organic semiconductors. *Chem. Rev.* **2007**, *107*, 926–952.
- (47) Coropceanu, V.; Sánchez-Carrera, R. S.; Paramonov, P.; Day, G. M.; Brédas, J. L. Interaction of charge carriers with lattice vibrations in organic molecular semiconductors: Naphthalene as a case study. *J. Phys. Chem. C* **2009**, *113*, 4679–4686.
- (48) Xie, X.; Santana-Bonilla, A.; Troisi, A. Nonlocal electron—phonon coupling in prototypical molecular semiconductors from first principles. *J. Chem. Theory Comput.* **2018**, *14*, 3752–3762.
- (49) Lee, M. H.; Troisi, A. Vibronic enhancement of excitation energy transport: Interplay between local and non-local exciton-phonon interactions. *J. Chem. Phys.* **2017**, *146*, 075101.
- (50) Giaimo, J. M.; Lockard, J. V.; Sinks, L. E.; Scott, A. M.; Wilson, T. M.; Wasielewski, M. R. Excited singlet states of covalently bound, cofacial dimers and trimers of perylene-3,4:9,10-bis(dicarboximide)s. *J. Phys. Chem. A* **2008**, *112*, 2322–2330.
- (51) McRae, E. G.; Kasha, M. Enhancement of phosphorescence ability upon aggregation of dye molecules. *J. Chem. Phys.* **1958**, 28, 721–722.
- (52) Kasha, M. Energy transfer mechanisms and the molecular exciton model for molecular aggregates. *Radiat. Res.* **1963**, 20, 55–70.
- (53) Kasha, M.; Rawls, H. R.; Ashraf El-Bayoumi, M. The exciton model in molecular spectroscopy. *Pure Appl. Chem.* **1965**, *11*, 371–392.
- (54) Bassler, H. Localized states and electronic transport in single component organic solids with diagonal disorder. *Phys. Status Solidi B* **1981**, *107*, 9–54.

- (55) Hestand, N. J.; Spano, F. C. Molecular aggregate photophysics beyond the kasha model: Novel design principles for organic materials. *Acc. Chem. Res.* **2017**, *50*, 341–350.
- (56) Hestand, N. J.; Tempelaar, R.; Knoester, J.; Jansen, T. L. C.; Spano, F. C. Exciton mobility control through sub-angstrom packing modifications in molecular crystals. *Phys. Rev. B: Condens. Matter Mater. Phys.* **2015**, *91*, 195315.
- (57) Kasha, M. Characterization of electronic transitions in complex molecules. *Discuss. Faraday Soc.* **1950**, *9*, 14–19.
- (58) Small, G. J. Herzberg-Teller Vibronic Coupling and the Duschinsky Effect. J. Chem. Phys. 1971, 54, 3300–3306.
- (59) Schreiber, M.; Toyozawa, Y. Numerical experiments on the absorption lineshape of the exciton under lattice vibrations. I. The overall lineshape. *J. Phys. Soc. Jpn.* **1982**, *51*, 1528–1536.
- (60) Schreiber, M.; Toyozawa, Y. Numerical Experiments on the Absorption Lineshape of the Exciton under Lattice Vibrations. II. The Average Oscillator Strength per State. *J. Phys. Soc. Jpn.* **1982**, *51*, 1537–1543.
- (61) Dimitriev, O. P.; Piryatinski, Y. P.; Slominskii, Y. L. Excimer emission in j-aggregates. *J. Phys. Chem. Lett.* **2018**, *9*, 2138–2143.